Microstructural investigation and identification of intermetallic σ-phase in solution annealed 316L-type austenitic stainless steel

Lescur, A.; Stergar, E.; Lim, J.; Hertelé, S.; Petrov, R. H.

DOI
10.1016/j.matchar.2021.111524

Publication date
2021

Document Version
Final published version

Published in
Materials Characterization

Materials Characterization 182 (2021) 111524

Contents lists available at ScienceDirect

Materials Characterization

journal homepage: www.elsevier.com/locate/matchar

Microstructural investigation and identification of intermetallic σ-phase in solution annealed 316L-type austenitic stainless steel

A. Lescur [a,b,*], E. Stergar [a], J. Lim [a], S. Hertelé [b], R.H. Petrov [b,c]

[a] Belgian Nuclear Research Centre (SCK CEN), Belgium
[b] Ghent University, Department of Electromechanical Systems & Metal Engineering, Belgium
[c] Delft University of Technology, Department of Materials Science and Engineering, the Netherlands

ARTICLE INFO

Keywords:
316L
Intermetallic σ-phase
Mechanical testing
Microstructure
EBSD
EDX

ABSTRACT

MYRRHA (Multi-purpose hYbrid Research Reactor for High-tech Applications) is an accelerator driven system, currently under development at SCK CEN in Mol, Belgium. This nuclear system will use liquid Lead-Bismuth eutectic alloy as a spallation target for fast neutron production and as coolant. The ideal structural material for a liquid metal cooled reactor should be unsusceptible to both liquid metal embrittlement and liquid metal corrosion, while possessing high toughness. Nuclear grade austenitic stainless steels similar to AISI 316L have therefore been chosen as the main candidate structural materials for MYRRHA. In the framework of the qualification of those candidates, a specific batch of this material has shown unexpectedly poor mechanical properties, which triggered the need of in-depth microstructural analysis. The behaviour was attributed to the unexpected and undesired presence of intermetallic σ-phase. The σ-phase was identified with a high confidence by combining the data for chemical composition from energy-dispersive X-ray spectroscopy and crystallographic information from electron backscatter diffraction by comparing simulated Kikuchi diffraction patterns with experimentally recorded ones. At first sight the optical appearance of σ-phase resembles δ-ferrite islands, which results in the risk of overlooking this when only classical material qualification methods are used. When left undetected, testing this material including the brittle σ-phase in a liquid metal environment, in combination with miniature mechanical test specimens, could lead to misinterpretation of embrittlement of the austenitic matrix.

1. Introduction

MYRRHA (Multi-purpose hYbrid Research Reactor for High-tech Applications) is an accelerator-driven system, currently under development at SCK CEN in Mol, Belgium [1] [2]. This nuclear system will use liquid Lead-Bismuth Eutectic (LBE) alloy as a spallation target for fast neutron production and as coolant. One of the main challenges to build MYRRHA is choosing suitable materials that can withstand the conditions imposed by the heavy liquid metal environment. Decades of earlier research has shown that some materials such as ferritic-martensitic steels are prone to liquid metal corrosion (LMC), embrittlement (LME) or both [3] in an LBE environment. The ideal structural material for a liquid metal-cooled reactor should be unsusceptible to both while possessing high toughness. Austenitic stainless steels similar to AISI 316L are currently the main candidate structural materials for MYRRHA.

Nevertheless, Ni-rich austenitic stainless steels with high amounts of Cr and Mo are also known to have a tendency to form a series of intermetallic phases such as Sigma (σ), Chi (χ) or Laves (η) phases or carbides like $M_{23}C_6$ or M_6C after long term exposure to a temperature range between 550 and 900 °C [4–11] or after post-weld heat treatments [12]. The most commonly found phase in the list above is the σ-phase. In general, the presence of those phases is to be avoided or kept at a minimum, due to their negative impact on ductility and fracture toughness. A reduction in impact energy and in reduction of area with an increased amount of σ-phase in austenitic steels is reported, where the absorbed impact energy drops from 75 J to 10 J in the case of fractions over 2% of σ-phase [12,13]. In addition, Cr- and Mo-rich phases deplete the Cr- and Mo-content in the neighbouring austenite matrix, locally decreasing the corrosion resistance of the material.

Sigma-phase has been known and studied for a long time and was first discovered as a pure Fe—Cr compound in 1907 by Treitschke and Tammann [14], who initially called it B-constituent due to its brittle nature. It was first observed in austenitic stainless steels in 1966 both by Hattersley and Hume-Rothery [15] and Hall and Algie [16] and has a

* Corresponding author at: Belgian Nuclear Research Centre (SCK CEN), Belgium.
E-mail address: amke.lescur@sckcen.be (A. Lescur).

https://doi.org/10.1016/j.matchar.2021.111524
Received 31 August 2021; Received in revised form 14 October 2021; Accepted 15 October 2021
Available online 20 October 2021

complex tetrahedral closed packed (t.c.p.) crystal structure with 30 atoms in its unit cell [4]. The structure has a body centred tetragonal Bravais lattice with a space group symmetry $P4_2/mnm$ and in 316L lattice parameters a = 0.87–0.92 Å and c = 4.554–4.8 Å [8,17]. Although many authors describe it as a pure Fe—Cr phase with an approximately even distribution of both elements, other compositions have been reported as well with a wide stoichiometric range. Besides the Fe- and Cr-atoms, also Mo-, Ni- and Mn-atoms can be present in the structure. For instance, Rhouma et al. found σ-phase with a composition of 0.8% Si, 35.8% Cr, 2% Mn, 50% Fe, 2.7% Ni and 8.7% Mo after an ageing treatment of 10,000 h at 650 °C on AISI 316L material [5]. The chemical composition of the phase depends on the formation mechanism and the chemical composition of the mother phase [6,7]. Sigma-phase can precipitate in different ways, initiating from austenite, from ferrite, at grain boundaries or from carbides, and since the diffusion process in solids is a slow process, on average the atoms will not diffuse back to the solid solution. Hence σ-phase precipitated at the γ/γ grain boundary will have a different composition compared to the σ-phase found after decomposition of δ-ferrite. This results in the argument that only the classical ternary Fe-Cr-Ni or Fe-Cr-Mo phase diagram is no longer satisfactory for predicting the possible presence of intermetallic phases in this case, based on the nominal composition alone, and local inhomogeneities play a crucial role.

The mechanisms of the σ-phase formation depend on chemical composition, duration and temperature of the ageing treatment, the thermodynamic state of the material or the microstructural features of the steel. The most favourable and most reported formation path after relatively short ageing times is the eutectoid decomposition of δ-ferrite into σ-phase and secondary austenite ($\delta \rightarrow \sigma + \gamma_2$), where the σ-phase forms at the phase boundary between ferrite and austenite [6,18]. After longer ageing times the σ-phase can also start to precipitate on γ/γ grain boundaries, twin boundaries, grain boundary triple junctions, or even in the interior of the austenite grains at very long ageing times. As an example, the combination of a full transformation of all δ-ferrite into σ-phase and secondary austenite, σ-phase precipitation at grain boundaries and precipitation on the interior of grains was found in 316L steel pipes after 100,000 h of operation at 640 °C by de Moraes et al. [7]. A partial reason for these different ways of formation at different timescales is that diffusion of the Cr and Mo alloying elements is faster in the ferritic b.c.c. lattice than in the austenitic f.c.c. lattice and therefore can occur faster and at lower temperatures [6]. Regarding the nucleation of such a phase, some claim that the initiation needs a carbide particle; others claim that the nucleation of the phase does not happen at the carbide particles. The presence of a high-energy interface is assumed to be necessary in some cases, like the δ/γ phase boundary or at later stages grain boundaries [19,20].

The material investigated in this study is a solution annealed nuclear grade 316L plate with no ageing treatment, therefore no presence of intermetallic phases is expected nor would be looked for. Phases resulting in unexpected poor mechanical properties of the 316L steel were located and identified as σ-phase. In practice, when σ-phase is expected in the material because of high-temperature working conditions, for example, the evolution of the fraction of σ-phase in the material is often monitored throughout time using magnetic techniques [13,21,22], where the decrease in magnetic signal is attributed to the transformation of magnetic δ-ferrite into non-magnetic σ-phase. However, when no σ-phase is expected, the standard procedure of qualifying material will not result in identification of σ-phase. Such qualifying procedures include tensile testing in rolling direction (L) or transversal direction (T), but not in the through-thickness direction (S), where the effect of σ-phase is most likely to be observed. Microstructural qualification is done by cross-sectional analysis using only classical etchants, which usually do not make the distinction between δ-ferrite and other phases. In this paper, we suggest a specific method to identify the presence of σ-phase in austenitic stainless steels in the qualification process. First, the indications for the σ-phase observed in mechanical tests will be discussed, after which the microstructural identification is shown. Both the mechanical testing of through-thickness specimens and the microstructural analysis including Kikuchi pattern simulation are tools for identifying the presence of σ-phase early in the qualification process.

2. Method

2.1. Material and mechanical properties

A plate of solution annealed 316L with a thickness of 30 mm was investigated. The nominal chemical composition of the material was obtained by Optical Emission Spectroscopy (OES) with a Spectro-SPECTROMAXx (www.spectro.com) metal analyser and is given in Table 1, together with the composition of some standard grades. According to European standards, the grade under investigation can be both identified as 1.4404 and as 1.4435 with a Cr, Mo and Ni content in the middle of both provided ranges, while American standards would call this an AISI 316L grade.

In the framework of qualifying candidate structural materials for LBE cooled systems, a mechanical testing program was employed, including slow strain rate tensile tests (SSRT). Uniaxial tensile test specimens were extracted along the three main axes of the plate and tested in air. All samples were tested at a slow strain rate of $5{\cdot}10^{-5}$ s^{-1}. Cylindrical tensile specimens were fabricated with a reduced parallel section of 12.0 mm and a gauge diameter of 2.4 mm. While standards for materials qualification typically only require tensile testing in the rolling (L) and transversal (T) orientation, in this study through-thickness (S) oriented tensile samples were also tested in air at room temperature. Fracture surfaces of those S-oriented specimen were thoroughly investigated by SEM and EDX using a JEOL JSM6610 system with a Bruker Quantax EDX detector.

2.2. Identification and characterization of intermetallic phase

To correctly identify the phases causing the poor mechanical behaviour, a combination of various techniques and methods was used in this work. To observe the distribution and character of intermetallic phases throughout the plate, metallographic samples were ground by SiC papers up to P2000 with subsequent diamond polishing of 6 μm, 3 μm and 1 μm. The metallographic samples were etched with different etchants (V2A and Murakami) and investigated by optical microscopy (OM) using a Keyence VHX-6000 digital light microscope. Images were taken over the whole cross section of the plate, which allowed for measuring the distribution of the phases as a function of the through-thickness position in the plate. The δ-ferrite content along the thickness position was determined using a Fisher Feritscope® FMP30C. Using the Feritscope®, the amount of ferromagnetic material in steel is measured, which includes δ-ferrite and martensite; however the latter seems unlikely to form in the material due to the high amount of Ni and other austenite stabilizing elements. The possible intermetallics (σ, χ, …) in the material are paramagnetic [13,21,22] and therefore cannot be quantified by this method. The used device is able to measure a δ-ferrite content in the range of 0.1 to 80%.

The microstructure, chemical composition and diffraction patterns of the intermetallic phase were investigated by SEM analysis using a JEOL JSM6610 system with Bruker Quantax EDX and Quantax EBSD detectors. The EBSD data was recorded and analysed using the Bruker Esprit software. Post-processing was done with MTeX, a freely available MATLAB toolbox for EBSD analysis [24]. Complementary, theoretical Kikuchi patterns were generated by kinematic simulation, using the Bruker Esprit software, and visually compared to experimental patterns, in order to ensure correct phase identification. This SEM/EBSD analysis was done on metallographic samples prepared in the same way as for the optical microscopy analysis but with an additional final polishing step using OP-S silica suspension.

Table 1
Composition of material used in this work (30 mm thick plate) determined by Optical Emission Spectroscopy (OES), compared with standard compositions of 316L-type steels.

	C (wt%)	Si (wt%)	Mn (wt%)	P (wt%)	S (wt%)	Cr (wt%)	Mo (wt%)	Ni (wt%)	N (wt%)	Fe
30 mm thick plate	0.022	0.52	1.10	0.029	0.008	17.1	2.52	12.4	0.08	Bal.
AISI 316L [23]	≤0.030	≤0.75	≤2.00	≤0.045	≤0.030	16.0–18.0	2.0–3.0	10–14	≤0.10	Bal.
1.4404 [23]	≤0.030	≤1.00	≤2.00	≤0.045	≤0.015	16.5–18.5	2.0–2.5	10.0–13.0	≤0.11	Bal.
1.4435 [23]	≤0.030	≤1.00	≤2.00	≤0.045	≤0.015	17.0–19.0	2.5–3.0	12.5–15.0	≤0.11	Bal.

3. Results

3.1. Mechanical test results

Engineering stress-strain curves of S-oriented specimen tested at room temperature in air with a strain rate of $5{\cdot}10^{-5}$ s^{-1} are shown in Fig. 1. One of the tested samples (A) shows the expected ductile stress-strain behaviour of 316L-type material. In the other tests the stress-strain curves are interrupted abruptly before reaching the maximum strength of the material. SEM images of the fracture surfaces of the tests indicated by A and B in Fig. 1 are shown in Fig. 2. The fracture surface of specimen A (Fig. 2a–b) shows a typical ductile fracture surface with dimples and local necking. The fracture surface of test B (Fig. 2c–d) shows a clearly different fracture behaviour. As can be seen from Fig. 2c and d, a mixed fracture with ductile and brittle features is observed.

Regions with only ductile features and with only brittle features were identified on the fracture surfaces shown (Fig. 2). Chemical analysis using EDX was performed on multiple zones for each type of fracture surface (as indicated by the * and ∘ on Fig. 2a and c) and the elements were quantified. The averaged data is summarized in Table 2. A higher Mo and Cr content is clearly observed in the brittle fracture surface, together with a depletion in Ni.

3.2. Identification of phases

For 316L-type materials the most obvious possible phase next to austenite is δ-ferrite. Therefore, the δ-ferrite content was measured by the Fisher Feritscope® FMP30C and the results are summarized in Fig. 3. A significant difference in δ-ferrite content is observed between the centre of the plate (0.28%) and both top and bottom (< 0.1%). Comparing these results with optical microscopy shows clear differences (see Fig. 3).

The top and bottom of the steel plate have a similar microstructural appearance regarding intermetallic phase content, where the non-austenitic phase content is higher in the centre of the plate compared to the sides. Stitched OM images were made across the full thickness of the plate with a width of approximately 5 mm to count the amount of non-austenitic phases. The plate was divided in sections of 2 mm of depth and for each section all intermetallic phases were counted and measured in area. Using these values, the area fraction of this phase is calculated as a function of the depth through the plate and is shown in the graph in Fig. 3. Clear segregation of the phase is present, agreeing with the observation in the δ-ferrite measurements in the centre and at the top/bottom of the plate, and resulting in a maximum area fraction of 0.9% in the centre.

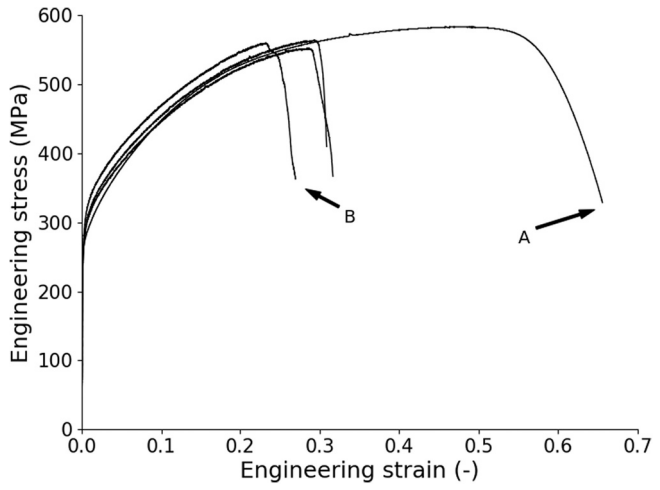

Fig. 1. Stress-strain curves of tensile tests performed with S-oriented specimen, tested at room temperature in air with a strain rate of $5{\cdot}10^{-5}$ s^{-1}. Indicated are the curves of tests (A, B) for which fracture surfaces are shown in Fig. 2.

In the centre of the plate, a maximum δ-ferrite content of 0.28% is measured while the maximum area fraction of non-austenitic stringers was calculated to be 0.9%. Around one third of the detected inclusions can hence be attributed to δ-ferrite, the other two thirds have to be attributed to something else. As other possible phases such as σ-phase or χ-phase are paramagnetic and cannot be detected by this measuring technique, the steel was analysed by additional chemical etching and OM. A cross-section of the material etched by V2A etchant is shown in Fig. 4. The OM images show the difference in non-austenitic phase content in the centre (4a) and near the top (4b) of the steel plate. As the V2A did not allow to unambiguously differentiate between σ-phase and δ-ferrite, an additional etchant was used to distinguish between the δ-ferrite and σ-phase. Murakami etchant [10] was used to differentiate between them and OM images after etching are shown in Fig. 5. While the austenite is not affected by the etchant, the σ-phase has a dark grey appearance and the δ-ferrite orange-brown colour.

To further confirm the identity of the additional phase as σ-phase, SEM analysis was performed. Backscattered electron SEM images of the phase are shown in Fig. 6. These images were taken on a cross section of the plate, with an orientation indicated on the image. The bright phase has a stringer-like appearance in some cases (Fig. 6a) and eutectic appearance in others (Fig. 6b). One of each type of appearance was further investigated with chemical (EDX) and crystallographic (EBSD) analysis.

EDX chemical mapping of the location with a high density of the phase with eutectic appearance is shown in Fig. 7. Chemical banding and segregation due to the rolling process of the steel is clearly visible by intensity difference due to locally varying contents of Mo, Cr, Ni or other elements present, as indicated with the white dotted lines in Fig. 7b. The areas around and on the position of the white appearing phases on the BSE images contain significantly higher concentrations of Mo and Cr compared to the matrix. This effect is most clearly visible for the Mo mapping.

EBSD measurements were performed on one of the phases with eutectic appearance indicated in Fig. 7 and the phase map is shown in Fig. 8a. The phase identification with the Bruker Esprit software indicated the phase as σ-phase, but with a pattern quality too low to be accepted. Due to this low confidence in the pattern and in order to ensure correct phase identification, additional visual comparisons were performed between the experimentally measured Kikuchi pattern (Fig. 8b) and a simulated theoretical pattern (Fig. 8c) of position A indicated on the phase map. The theoretical diffraction pattern was generated based on the crystallographic structure of the suspected σ-phase and its specific orientation towards the electron beam and detector. The simulated pattern not only shows the location and width of

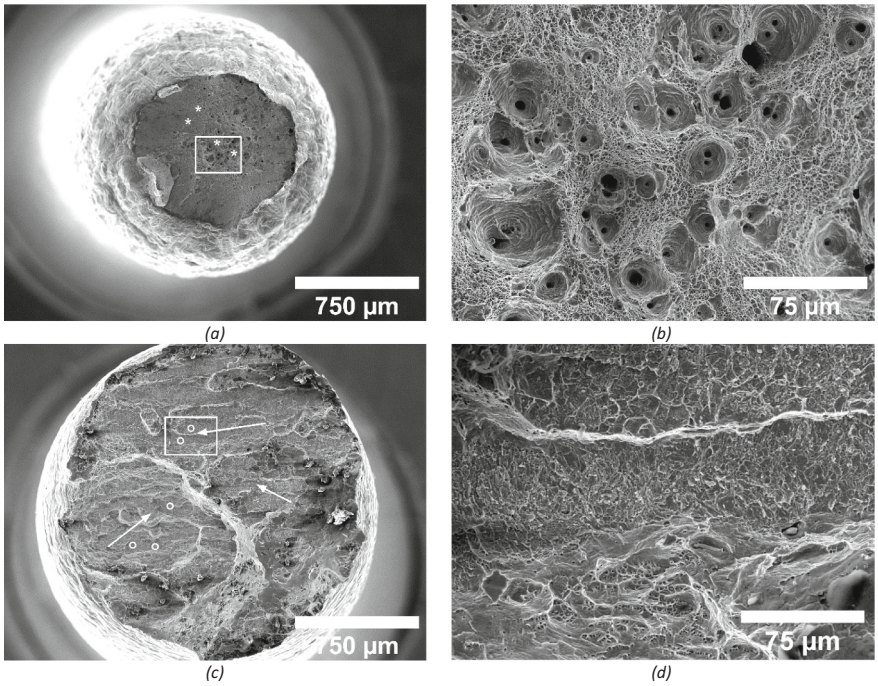

Fig. 2. Fracture surfaces of tested samples extracted in S-orientation indicated in Fig. 1. (a) overview of sample A, (b) detail out of (a) indicated by the box, (c) overview of sample B and (d) detail out of (c) indicated by the box. The arrows in (c) indicate regions with brittle fracture and the stars in (a) and circles in (c) mark points for EDX.

Table 2
Averaged results of EDX measurements for ductile and brittle area measured on indicated positions in Fig. 2a and c on S-oriented fracture surfaces.

	Si (wt %)	Cr (wt %)	Mn (wt %)	Fe (wt %)	Ni (wt %)	Mo (wt %)
Ductile area (*)	0.3	17.3	2.3	66.5	11.4	2.2
Brittle area (○)	0.5	25.7	1.6	58.8	6.3	7.1

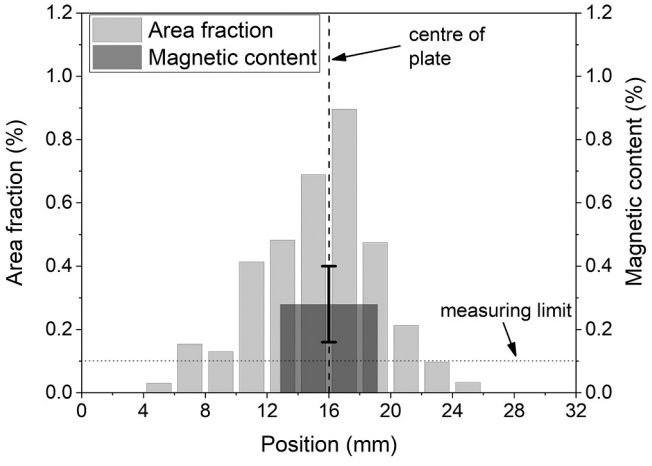

Fig. 3. Comparison of the measured area fraction of stringers (measured by optical microscopy) and the δ-ferrite content (measured by Feritescope) as function of the position in plate. The dashed vertical line marks the centre of the plate. The given values of the ferrite content represents the average of 10 measurements, with indicated one standard deviation interval.

the bands but also the relative intensity. As can be seen in Fig. 8, very good agreement was found between the simulated and experimental Kikuchi-pattern of the σ-phase. All theoretical higher order Kikuchi bands could be located on the experimental pattern and vice versa. However, the software identified some pixels on the map, located at a grain boundary between austenitic grains, as Laves-phase, but a more detailed analysis showed that they were wrongly indexed. The experimental and simulated pattern (shown in Fig. 8d and e) of position B indicated on the phase map are not compatible. Some clearly visible Kikuchi bands on the experimental pattern (indicated in red) are not present on the simulated pattern. This misindexation can be attributed to the resolution of the electron beam, when falling on a grain boundary between two austenite grains, leading to mixed signals of the adjacent grains, resulting in a combined pattern of Kikuchi-bands. Patterns recorded in both neighbouring grains (position C and D) are given in Fig. 8f and g, so the Kikuchi lines indicated in Fig. 8d can be explained.

A second region, where the to-be-identified phase is located on a grain boundary, without eutectic appearance, has been analysed using both EDX chemical mapping and EBSD phase identification (Fig. 9). On this stringer, the larger part could be identified with high confidence as δ-ferrite, while σ-phase is observed at the interface between the austenite and δ-ferrite. Also here targeted comparison of experimental and simulated Kikuchi patterns confirmed the identified σ-phase. The chemical mapping with the EDX technique shows differences in Mo-content between the σ-phase and the δ-ferrite.

4. Discussion

The previous section showed clear indications of σ-phase presence, both based on the observed fracture surfaces and microstructural analysis. Having identified this detrimental phase, the question is raised how it was formed in the material at hand. Similar appearing fracture surfaces as in Fig. 2c–d, with brittle zones of similar sizes were reported by Tseng et al. [9] after 20 h of annealing treatment at 720 °C of through-thickness tensile samples of 304 L steel, which was attributed to the formation of σ-phase after the ageing. The authors reported only a lower

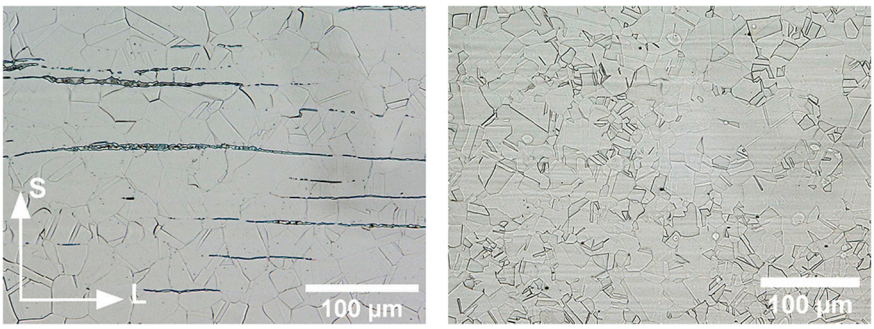

Fig. 4. Optical images after etching (V2A) of the centre (a) and top (b) of the plate. Orientation of the cross sections are the same for both images and are indicated in (a).

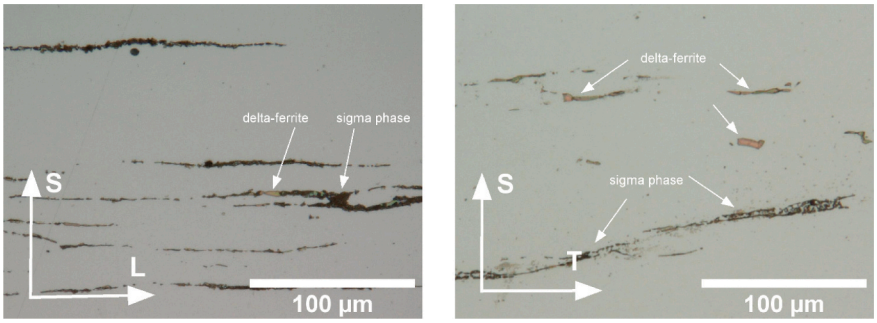

Fig. 5. Optical images after etching (Murakami etchant) of centre of plate in the (a) SL orientation and (b) ST orientation.

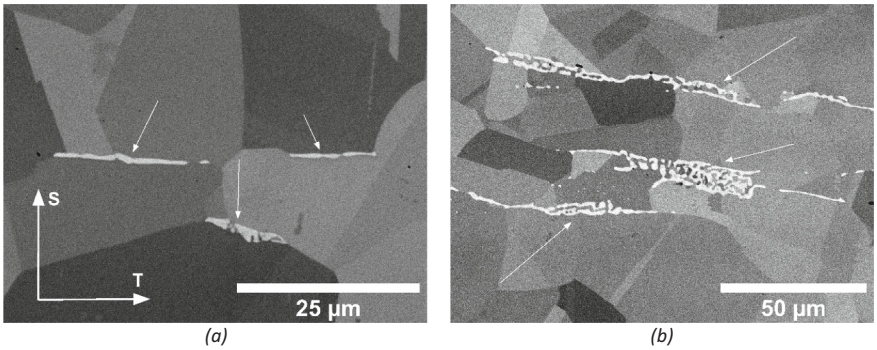

Fig. 6. SEM images using backscattered electron signal, the bright regions marked with arrows represent possible intermetallic σ-phases. Orientations within the plate is equal for both images and indicated in (a).

reduction of area (RA) but similar strength of the material tested while in our case the strength is also significantly reduced. At first sight, there is no apparent reason for the formation of σ-phase in the solution annealed 316L, which had no additional heat treatments. Other authors have encountered similar issues in the past [11,25] where no apparent reason existed for the formation of σ-phase. It was argued that the evolution of steel fabrication towards continuous casting could influence the quality of the annealing step and that the material was not well homogenized before further processing. Marin et al. studied the possible formation of σ-phase during the last stage of solidification and found σ-phase could be formed directly after chemical segregation of Cr or Mo in the remaining liquid [18]. Both a eutectic reaction at the last stage of solidification due to segregation of Mo in the remaining liquid ($L \rightarrow \gamma + \sigma$) and a eutectoid decomposition of δ-ferrite with a solid-state phase transformation ($\delta \rightarrow \sigma + \gamma_2$) are reported. For the second example in this paper (Fig. 9), the eutectoid decomposition of δ-ferrite is most likely, however for the first example (Fig. 8) both paths could have been the case.

In addition, the composition of the steel batch with high Cr and Mo-content used in this work creates a condition where, after chemical segregation, variations in composition can makes the formation of the σ-phase more likely in the zones with locally elevated Cr and Mo content. As can be observed in Table 1, different names can be attributed to the grade of steel, even within one family of standards such as the European standard. Both 1.4404 and 1.4435 can be used to describe the alloy. Within the ranges of the alloying content, this means that an alloy with a Cr-content of 16.5 w% or 19.0 w% can both be included in the same grade of steel as the one under investigation. The ranges suggested in the American standard AISI 316L are chosen even wider for some elements within one grade of steel. When looking at the ternary Fe-Cr-Mo system, the difference of 16.5 w% or 19.0 w% Cr can already have a large influence regarding intermetallic phase content. Therefore it is of

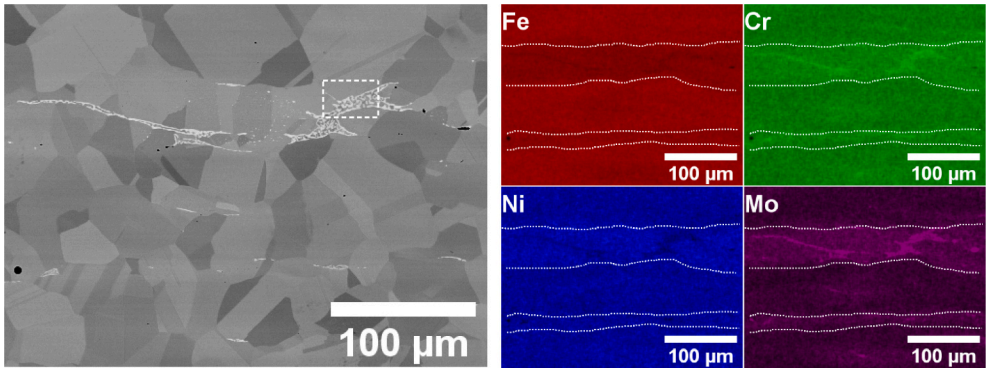

Fig. 7. (a) SEM image using backscatter signal of zone with high density of intermetallic phase precipitation. The white rectangle indicates the location for further EBSD analysis shown in Fig. 8. (b) Fe, Cr, Ni and Mo chemical mapping with dotted lines indicating micro-segregation.

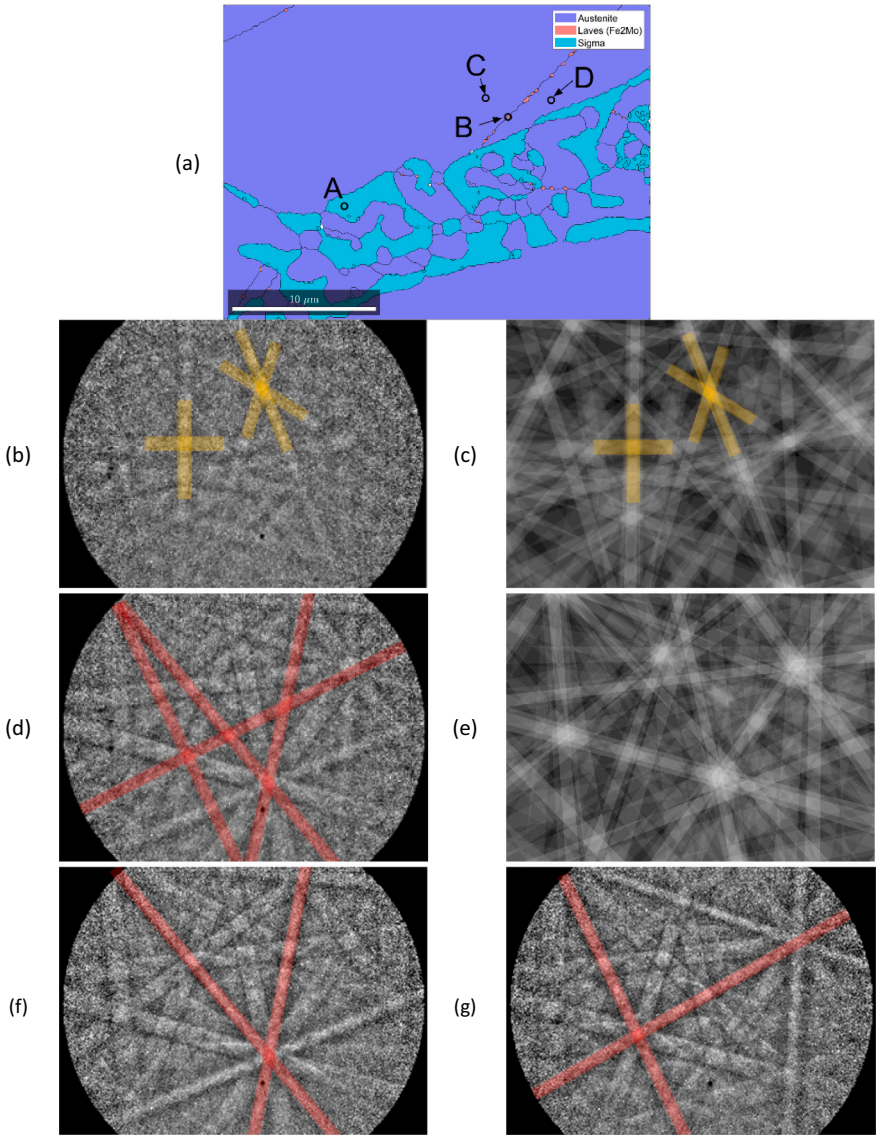

Fig. 8. (a) An EBSD phase map of the location indicated in Fig. 7a. Experimental Kikuchi patterns were recorded at points A, B, C and D. The experimental pattern of point A (b) was identified as σ-phase by the software and a simulated Kikuchi pattern of that position for the given indexed orientation and phase is given in (c). Reference lines are indicated in yellow as visual help. Similar experimental (d) and simulated (e) Kikuchi-patterns, recorded at position B are shown, where the experimental pattern was incorrectly identified as Laves-phase. Lines not visible on the simulation but clearly present in the recorded pattern are indicated in red. Diffraction patterns recorded in the neighbouring austenitic grains (C and D) are shown in (f) and (g), clarifying the origin of the red lines in (d). (For interpretation of the references to colour in this figure legend, the reader is referred to the web version of this article.)

high importance to report the actual chemical composition of materials worked with.

The assumption that chemical segregation contributes to the formation of σ-phase is of interest to our material, given the clear segregation present at mid-thickness of the plate (last part to solidify). Looking at both the magnetic measurements (Fig. 3) and the optical

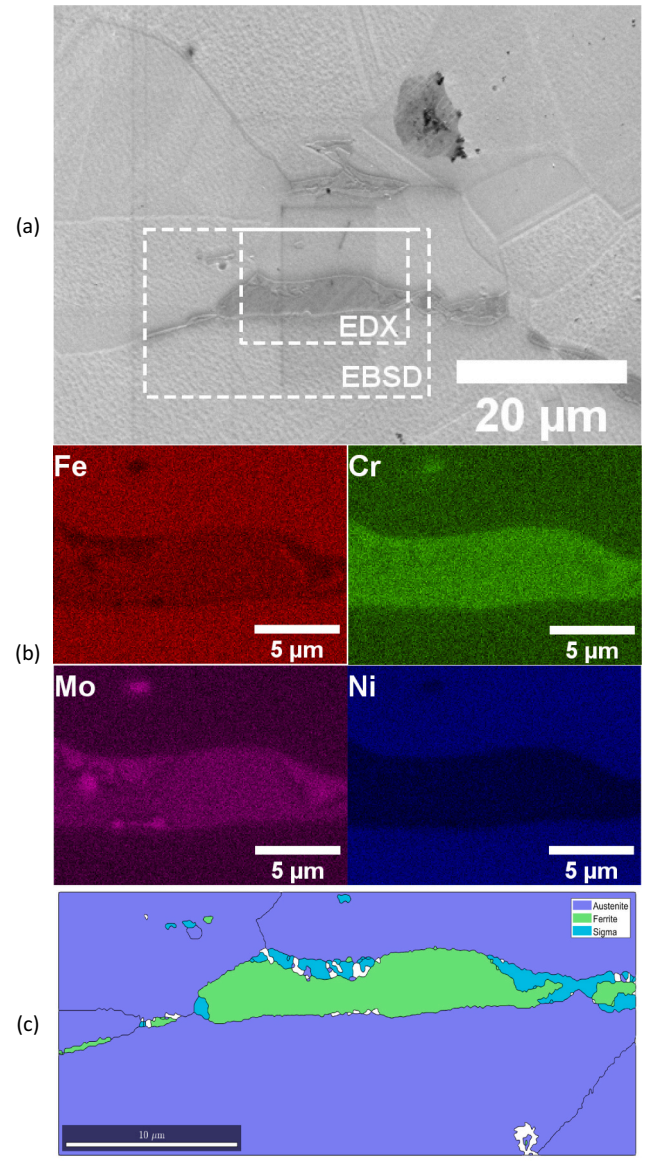

Fig. 9. (a) SEM image with indicated the locations of EDX chemical maps shown in (b) and EBSD phase map shown in (c).

measurements (Fig. 4) there is an increase in intermetallic phases and δ-ferrite stringers in the centre of the plate, falling to a content of zero towards the surface. Upon hot rolling, the plate will initially cool faster at the top and bottom, where a more equilibrium chemical composition for the austenite might be attained, leading to an excess of ferrite stabilizing elements (Cr, Mo) moving to the centre of the plate, in the remaining liquid phase. The higher Cr and Mo content increases the possible formation of σ-phase and its stability, as can be seen in the binary (and ternary) Fe-Cr(—Mo) phase diagrams found in literature [8]. Those local increases of Mo and Cr –as observed in Fig. 7– may trigger the formation of σ-phase.

The main issue in this matter is that σ-phase can remain undetected, since the microstructure (when not analysed in depth) looks very similar to what is expected, namely an austenitic matrix with stringers, suspected to be δ-ferrite. With only classical etchants and no EBSD measurements one would overlook the σ-phases, and this can have significant implications later on when the steel is in use. The σ-phase formation after ageing in service is known and will be looked for, but when an initially contaminated batch of 316L is used in an environment below these temperatures, there is a large likelihood that no one would suspect the formation of σ-phase.

5. Summary and conclusions

In a batch of 316L/1.4435 steel with high Cr, Ni and Mo content, next to the expected austenite and δ-ferrite, an additional intermetallic phase was found and successfully identified as σ-phase. The observed brittle behaviour in tensile tests was attributed to this undesired phase. In this work, a combination of microstructural analysis, magnetic detection of δ-ferrite and mechanical testing allowed for a successful identification of the unexpected phase. The comparison of the experimental and simulated diffraction patterns resulted in identifying the additional phase present in the material as σ-phase. The indexation reliability was higher than the one provided by the used commercial EBSD software.

Because of the apparent similar microstructure between the δ-ferrite and σ-phase stringers, when not analysed in depth, the unexpected σ-phase can remain undetected. In-depth EBSD analysis and mechanical testing in through-thickness orientations have proven to help solving this issue, where classical etchants and standard oriented tensile samples fall short. Adding those techniques to the standard qualification procedures for these specific steel grades is strongly recommended.

Although the σ-phase is in the least detrimental orientation in the plate to influence the structural integrity of a construction, care should still be taken to detect this type of characteristic in steel plates prone to the formation of such intermetallic phases. Even small amounts of intermetallic phases, when having deleterious orientation or geometry, can have an enormous effect on the properties of the steel. Using small scale samples the tested volume becomes an issue; however in this case this is what triggered further investigation of the problem.

Data availability

The raw/processed data required to reproduce these findings cannot be shared at this time as the data also forms part of an ongoing study.

Declaration of Competing Interest

The authors declare that they have no known competing financial interests or personal relationships that could have appeared to influence the work reported in this paper.

Acknowledgements

The research leading to these results has been carried out in the frame of EERA Joint Programme on Nuclear Materials and is partially funded by the European Commission HORIZON 2020 Framework Programme under grant agreement No. 755269. The work is also supported and partially funded by the Belgian government through the MYRRHA project. The authors would like to sincerely thank Y. Florenty for help with sample preparations and J. Joris, J. Bouwens and B. Geyskens for their technical support and performing the mechanical tests, their help is greatly appreciated.

References

[1] H.A. Abderrahim, P. Baeten, D.D. Bruyn, R. Fernandez, MYRRHA – a multi-purpose fast spectrum research reactor, Energy Convers. Manag. 63 (2012) 4–10.
[2] D.D. Bruyn, H.A. Abderrahim, P. Baeten, P. Leysen, The MYRRHA ADS project in Belgium enters the front end engineering phase, Phys. Procedia 66 (2015) 75–84.
[3] NEA, Handbook on Lead-bismuth Alloy and Lead Properties, Materials Compatibility, Thermal Hydraulics and Technologies, OECD, 2015.
[4] C. Hsieh, "Overview of Intermetallic Sigma (σ) Phase Precipitations in Stainless Steels," International Scholarly Research Notices, 2012.
[5] A.B. Rhouma, T. Amadou, H. Sidhom, C. Braham, Correlation between microstructure and intergranular corrosion behavior of low delta-ferrite content AISI 316L aged in the range 550-700 °C, J. Alloys Compd. 708 (2017) 871–886.
[6] D.M.E. Villanueva, F.C.P. Junior, R.L. Plaut, A.F. Padilha, Comparative study on sigma phase precipitation of three types of stainless steels: austenitic, superferritic and duplex, Mater. Sci. Technol. 22 (2006) 1098–1104.

[7] F.P. Moraes, S.F. Alves, R.L. Plaut, A.F. Padilha, Degradation of microstructure and properties of an AISI 316L steel pipe after more than 100,000 hours usage at 640 °C in a petrochemical industry, Procedia Structural Integrity 17 (2019) 131–137.
[8] A. Padilha, Decomposition of austenite in austenitic stainless steels, ISIJ Int. 42 (2002) 325–327.
[9] C.C. Tseng, Y. Shen, S.W. Thompson, M.C. Mataya, G. Krauss, Fracture and the formation of sigma phase, $M_{23}C_6$, and austenite from delta-ferrite in an AlSl 304L stainless steel, Metall. Mater. Trans. A 25 (1994) 1147–1158.
[10] G. Vander Voort, G.M. Lucas, E.P. Manilova, Metallography and microstructures of stainless steels and maraging steels, ASM Handbook 9 (2004) 670–700.
[11] X. Tang, Sigma phase characterization in AISI 316 stainless steel, Microsc. Microanal. 11 (2005) 78–79.
[12] S. Kozuh, M. Gojic, L. Kosec, Mechanical properties and microstructure of austenitic stainless steel after welding and post-weld heat treatment, Kovove Materialy - Metallic Materials 47 (2009) 253–262.
[13] E. Macedo Silva, J.P. Leite, J.P. Leite, W.M.L. Fialho, V.H.C. Albuquerque, J.M.R. S. Tavares, Induced magnetic field used to detect the sigma phase of a 2205 duplex stainless steel, Journal of Nondestructive Evaluation 35 (2016).
[14] W. Treitschke, G. Tammann, LIII. Über die Legierungen des Eisens mit Chrom, Z. Anorg. Chem. 55 (1907) 402–411.
[15] B. Hattersley, W. Hume-Rothery, The Constitution of Certain Austenitic Steels, 1966.
[16] E.O. Hall, S.H. Algie, The sigma phase, Metallurgical Reviews 11 (1966) 61–88.
[17] H.L. Yakel, Atom distribution in sigma phases. I. Fe and Cr atom distribution in a binary sigma phase equilibrated at 1063, 1013 and 923 K, Acta Crystallographica Section B 39 (1983) 20–28.
[18] R. Marin, C. Hervé, J. Zollinger, M. Dehmas, B. Rouat, A. Lamontagne, N. Loukachenko, L. Lhenry-Robert, σ-Phase formation in super austenitic stainless steel during directional solidification and subsequent phase transformations, Metallurgical and Materials Transactions A 51 (2020) 3526–3534.
[19] B. Weiss, R. Stickler, Phase instabilities during high temperature exposure of 316 austenitic stainless steel, Metall. Mater. Trans. B 3 (1972) 851–866.
[20] Y.S. Sato, H. Kokawa, Preferential precipitation site of sigma phase in duplex stainless steel weld metal, Scr. Mater. 40 (1999) 659–663.
[21] E.A. Huallpa, E.F. Monlevade, J.C. Sánchez, M.A. Campos, L. Padovese, H. Goldenstein, Use of magnetic Barkhausen noise (MBN) to follow up the formation of sigma phase in saf2205 (UNS S31803) duplex stainless steel, Mater. Res. 19 (2016) 1008–1016.
[22] S.S.M. Tavares, J.M. Pardal, J.L. Guerreiro, A.M. Gomes, M.R. Silva, Magnetic detection of sigma phase in duplex stainless steel UNS S31803, J. Magn. Magn. Mater. 322 (2010) L29–L33.
[23] C. Wegst, M. Wegst, Key to Steel, 2010.
[24] F. Bachmann, R. Hielscher, H. Schaeben, Grain detection from 2d and 3d EBSD data — specification of the MTEX algorithm, Ultramicroscopy 111 (2011) 1720–1733.
[25] S.F. Bordín, S. Limandri, J.M. Ranalli, G. Castellano, EBSD spatial resolution for detecting sigma phase in steels, Ultramicroscopy 171 (2016) 177–185.